PAPER • OPEN ACCESS

Simulation and comparative analysis of Fiber Optic Gyroscope for near-zero rotation rate measurement

To cite this article: Mohamed N. Shalaby *et al* 2024 *J. Phys.: Conf. Ser.* **2847** 012004

Journal of Physics: Conference Series **2847** (2024) 012004 doi:10.1088/1742-6596/2847/1/012004

Simulation and comparative analysis of Fiber Optic Gyroscope for near-zero rotation rate measurement

Mohamed N. Shalaby[1,†,*], Ahmed H. Elghandour[2,†] and Mohamed Abdo M.[1,†]

[1] Engineering Physics Department, Military Technical College,Cairo, Egypt
[2] Communication Department, Military Technical College,Cairo, Egypt

Email : Mohamedshalaby5599@mtc.edu

† These authors contributed equally to this work.

Abstract. Currently, Fiber-Optic Gyroscopes (FOGs) stand as a significant leap in inertial navigation sensor technology within the field of automation, control and navigation. There has been a recent global emphasis on exploring and enhancing high-precision Inertial Navigation Systems (INS), focusing on the pivotal role of fiber optic gyros as a fundamental sensor. FOGs are leading in many aspects over the mechanical gyros which were used before in earlier decades as they are lighter in weight, require no moving parts in operation, with higher sensitivity, and quicker in both start-up and warm-up procedures. In our present work we will investigate the performance of FOG under a distinct operational condition—namely, Near-Zero Rotation Rate for both basic and phase modulation configurations. We will use OptiSystem software package to simulate both configurations and show the initial challenges encountered during the simulation and detailed how subsequent phases effectively addressed these issues and pointing out the significant conclusion.

1. Introduction

The essential growing need for inertial navigation sensors in places where Global Positioning System (GPS) isn't available or is limited as in indoor navigation, tunnels, caverns, etc. Earlier, mechanical gyros were once considered suitable as they use angular momentum to calculate rotational speed, but their reliance on moving parts, long warm-up times, high expenses, and lack of reliability have rendered them insufficient for many modern applications. While, FOG lack of rotating components is a key advantage over mechanical counterparts that is the main reason for their longevity. To address this, researchers have developed optical gyros employing lasers and fibres, which showed a significantly enhanced performance compared to their mechanical counter parts [1]. Sagnac effect Established by French physicist Sagnac in 1913 stated that "There will be a phase shift between two counter propagating waves due to rotation of the medium where they propagate" [2] formed the fundamental basis for all optical gyros.

FOG uses two light beams propagate concurrently along an optical fiber channel to detect angular velocity. As the plane of the optical fiber rotates, it induces a phase mismatch between the

two beams, directly correlated to the rotational velocity, which is known as the Sagnac effect. This effect is further utilized as light waves reach a photoelectric sensor, generating a current directly proportional to their intensity. The phase shift between the beams can be calculated from the detected optical power. Consequently, the rotation rate is deduced from the Sagnac formula [2] [3] [4]. There are two well-known primary types of optical gyros: (1) Ring Laser Gyroscopes (RLGs) and (2) Fiber Optic Gyroscopes (FOGs) [5]. Notably, the FOG's robustness stands out as a significant advantage caused by their independence on moving parts [6] [7], distinguishing it from competitors like mechanical gyros and RLGs (the latter employ dithering). Given these distinct advantages [8] [9], the FOG is poised to assume a crucial role in both military and commercial markets [10] [11]. Its recent surge in popularity within defense applications can be attributed to several factors, including its compact size, affordability, lightweight design, broad dynamic range, low power consumption, and the capability for batch production.

Gyroscopes are categorized into three main classes based on their precision and sensitivity: (1) Control Grade Gyroscopes that are capable of measuring rotation rates within the range of 10 to 100 degrees per hour. They are primarily used in applications where moderate precision is required for control systems. (2) Tactical Grade Gyroscopes that offers improved sensitivity compared to control grade ones, measuring rotation rates between 0.1 and 10 degrees per hour. They find application in scenarios demanding higher precision, such as navigation in various terrestrial and aerial systems. (3) Inertial Grade Gyroscopes that is the most sensitive type of gyroscope, capable of measuring rotation rates lower than 0.01 degree per hour. These gyroscopes are highly precise and are extensively utilized in space applications, where extreme precision and accuracy are crucial for navigation and orientation control in satellites and spacecraft [10].

OptiSystem is indeed a valuable simulation program for modeling and assessing the behavior of optical systems. Utilizing OptiSystem to conduct FOG simulation to illustrate the challenges encountered in the basic configuration of FOGs, highlighting the previously discussed problems. Additionally, OptiSystem can be employed to demonstrate how the phase modulated FOG resolves these issues, show casing its efficacy as a solution. Simulations serve as an excellent visual aid in understanding the performance differences and the effectiveness of various configurations.

2. Basic configurations of fiber optic gyros

In Figure1, illustrates the basic configuration of FOG, which includes a light source, a 3-dB optical coupler for splitting light into two beams that are then introduced to the single mode fiber coil, with each beam entering the coil from opposite terminals of the coil. The two beams rotate in a counter manner, and finally the emerging beams resultant interference is captured by the detector.

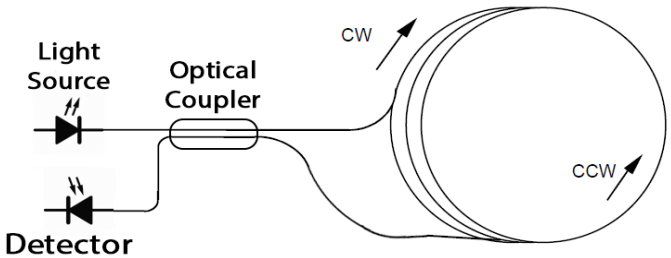

Figure 1. Basic FOGs Configuration

Figure 2 illustrates the relation between the detected power and the phase shift caused by the interaction between the two counter-propagating beams. This phase shift occurs as a consequence of the medium's rotation, as indicated in equation1

$$I = \frac{I_0}{2}[1 + cos(\Delta\phi_s)] \quad (1)$$

Where: I is the detected intensity, I_o is the input intensity and $\Delta\varphi_s$ is the sagnac phase shift due to rotation [5].

And the relation between the rotation rate and the induced phase shift between the counter propagating waves can be calculated using Sagnac formula as shown in equation 2 [12] [13] [14]

$$\Delta\phi_s = [2\pi LD/\lambda c] * \Omega \quad (2)$$

Where: L is the fiber length, D is the fiber ring coil diameter, λ is the light wavelength, c is the speed of light, and Ω is the rotation rate.

As shown in figure 2, there are two significant issues which limit the performance of the optical gyros. First, the low sensitivity at extremely low rotation rates, as in such low rates the detected power closely resembles the power observed at a phase shift of zero suggesting an apparent absence of rotation, even in situations where rotation does occur. This issue is particularly critical in applications such as submarines and space missions, where rotation rates are exceptionally minute, leading to minimal phase shifts. Consequently, the basic configurations may not be suitable for these applications.

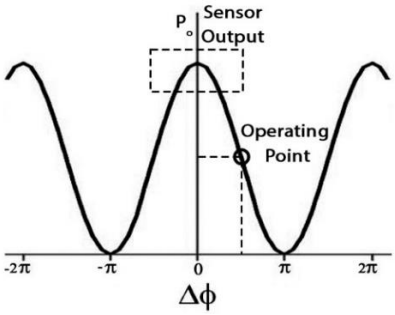

Figure 2. Relation between phase shift and detected power

The second issue that is highlighted in figure 2 is the inability to determine the direction of rotation using the basic configurations. This becomes apparent when observing identical detected powers for phase shifts as π/2 and -π/2. Despite these two phase shifts representing distinct opposite rotation directions, their corresponding detected powers remain the same within the basic configurations, rendering it impossible to discern the direction of rotation.

3. Phase modulated FOGs

The desired outcome from using a phase modulation in FOG is illustrated in figure 2. Where the objective is to shift the zero point, originally situated at zero phase shift where the maximum output power is detected, to any desired point, particularly targeting the high slope regions of the figure (operating point at figure 2 around π/2 where the relation between the phase shift and the detected optical power exhibits its maximum slope).

The phase modulated FOGs configuration is illustrated in figure 3. This configuration mirrors the basic configuration of FOGs in light source, coupler, single mode fiber coil and detector, with the inclusion of supplementary components such as a phase modulator, as a piezoelectric transducer, a sine generator with defined frequency and an electrical circuit as lock-in amplifier which collect the interfered modulated signals that is an indication of the targeted rotation rate. To realize this configuration, we first need to address the limitations encountered in the basic configurations which ca be calculated using the following mathematical model.

After phase modulation, equation 1 becomes:

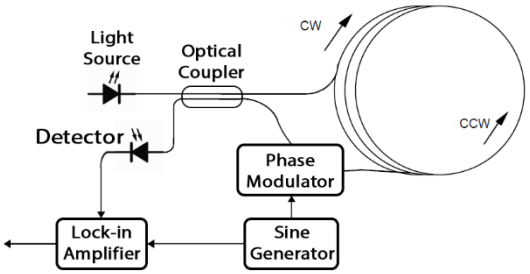

Figure 3. Phase Modulated FOGs Configuration amplifier

$$\langle I\rangle = \frac{I_0}{2}[1 + cos(\Delta\phi_s + \Delta\phi_m)] \tag{3}$$

Where: I is the detected intensity, I_0 is the intensity at no rotation, $\Delta\phi_s$ is the sagnac phase shift and $\Delta\phi_m$ Is the phase shift due to phase modulation.

$$\Delta\phi_m(t) = \phi_m(t) - \phi_m(t-\tau) \tag{4}$$

τ is the required time for beam to pass the fiber coil = [nL/c] where n is the refractive index, L is the fiber coil length and c is the speed of light in free space Thus, the interference signal becomes

$$\langle I\rangle = \frac{I_0}{2}[1 + cos(\Delta\phi_s + \Delta\phi_m) \tag{5}$$

The general form of the modulating signal is

$$\phi_m(t) = \phi_m cos(\omega_m t) \tag{6}$$

Where: ϕ_m is modulation depth and $\omega_m$is the modulation frequency

$$\Delta\phi_m(t) = \phi_m[cos(\omega_m t) - cos(\omega_m t - \omega_m \tau)] \tag{7}$$

Setting $\omega_m\tau$= π Thus,

$$\Delta\phi_m(t) = 2\phi_m cos(\omega_m t) \tag{8}$$

Returning to the detector signal

$$\langle I\rangle = \frac{I_0}{2}\{1 + cos(\Delta\phi_S)\, cos[\Delta\phi_m(t)] - sin(\Delta\phi_S)\, sin[\Delta\phi_m(t)]\} \tag{9}$$

We can solve it by using Bessel function of the first kind, we find

$$\begin{aligned}\langle I\rangle = \frac{I_0}{2}\{1 + cos(\Delta\phi_S)[J_0(2\phi_m) + 2\textstyle\sum_{n=1}^{\infty}\ (-1)^n J_{2n}(2\phi_m)cos(2n\omega_m t)] \\ +2sin(\Delta\phi_S)\textstyle\sum_{n=1}^{\infty}\ (-1)^n J_{2n-1}(2\phi_m)\, cos[(2n-1)\omega_m t]\}\end{aligned} \tag{10}$$

For the detector output signal, the first term represents the near-zero rotation rate component, while the second term signifies the first harmonic, followed by subsequent harmonics. Despite all harmonics appearing in the output of the detector, our requirement is solely for the first harmonic (at the used frequency), precisely as described in equation11. This first harmonic encompasses the necessary phase information (Sagnac phase), crucial for the computation of the rotation rate, as discussed earlier. Absolutely, the lock-in amplifier serves the purpose of detecting this signal effectively. By utilizing a reference signal at the modulating frequency, this amplifier can isolate and extract the detected signal precisely at that same frequency. Within this signal lies the crucial data pertaining to the phase shift between the counter-propagating waves, enabling accurate analysis and utilization for the intended purpose.

Indeed, when selecting the phase modulator depth to be +/-0.9 radians, the corresponding term Φo = 0.9 results in the value for the Bessel function J1(2Φo) = 0.581517 being maximized.

This specific value of the Bessel function is attained when the phase modulation depth is set at +/- 0.9 radians.

$$I_\omega = I_o 2J_1(2\Phi o)sin(\phi_s) \tag{11}$$

Where: $I_\omega$is the required intensity (intensity at modulation frequency), $I_o$intensity at no rotation, Φo is the modulation depth and $\phi_s$is Sagnac phase shift. We chose this factor from Bessel equation as it contains the required rotation rate as the rotation rate is very small so sagnac phase shift is very small so, $sin(\phi_s) = \phi_s = [2\pi LD/\lambda c] * \Omega$as mentioned in equation 2 so, we can detect the rotation rate Ω.Absolutely, maximizing the detected signal at the modulating frequency ω_m simplifies the process of determining the rotation rate using equation10. This optimization ensures that the signal containing the necessary phase information is heightened and easily discernible, streamlining the calculation of the rotation rate through the established equation.

4. Simulation results and discussion

We will conduct a comprehensive comparison, analyzing the results from both the near-zero rotation rate simulation of the basic FOGs configuration and the phase modulated FOG configuration. Simulation will provide a clear contrast, especially regarding small rotation rates and the determination of rotation directions. This comparison will effectively demonstrate the advantages of the phase modulated configuration over the near-zero rotation rate setup in terms of sensitivity and directional discernment at minimal rotation rates.

4.1. Basic FOGs configuration

The figure 4 illustrates the simulation of a basic FOGs configuration which consisting of light source of input power1 mW, two 3 dB couplers, two 500 m fiber coils, and a photodiode utilized for power detection.

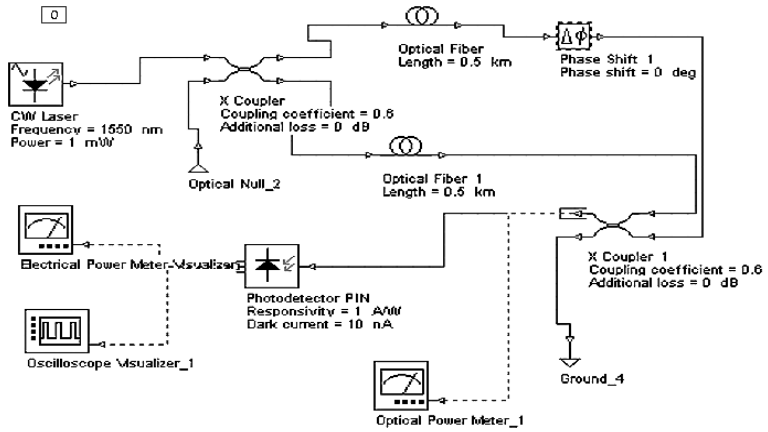

Figure 4. Simulation of Basic FOGs Configuration

In this simulation, the principle of reciprocity was maintained by employing two identical fiber coils, ensuring they possess identical properties within the system. We introduced a variable phase shift module to act as a replacement for the rotation of the system. By conducting iterations across phase shifts ranging from -180 to 180 degrees in the simulation, you established a comprehensive dataset. Plotting this data enabled the visualization of the relationship between detected power and phase shift, aligning with the pattern described by equation 1. This method helps to validate the theoretical model through simulated results as shown in figure 5.

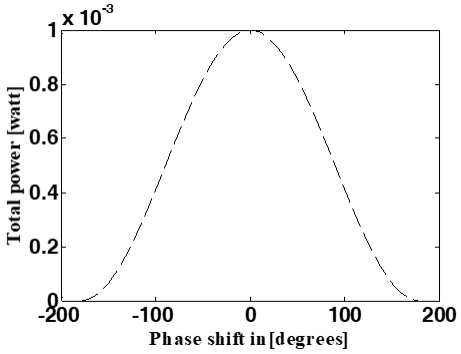

Figure 5. Simulation result of Relation between Phase Shift and Detected Power for Basic GOFs Configuration

Table 1 shows the results of the simulation done on the Basic FOGs Configuration, for the detected power at these low rotation rates closely resembles the detected power at zero phase shift. Which shows in a clear way the very slight variation of the detected power which emphasize the gyro's inability to differentiate between these extremely low rotation rates and a stationary state, which is exactly the first limitation of the basic FOGs configuration stated before.

By analyzing specific phase shifts and their corresponding values with opposite signs, we've discovered that despite this sign difference, their detected powers remain identical. This observation confirms the second limitation for the basic configuration, namely its inability to distinguish the direction of rotation. This phenomenon emphasizes the challenge in determining the rotational direction based solely on detected power readings as will be shown in table 2

Table 1. Comparison between detected power at low phase shifts around zero at basic configuration and phase modulated FOGs.

Phase Shift (deg)	Detected Power for Basic FOGs Configuration (uW)	Detected Power for Phase Modulation FOGs Configuration (uW)
0	960	518.1
0.5	959.98	520.33
1	959.92	5.22.56
1.5	959.85	524.9
2	959.72	527
2.5	959.55	529.23
3	959.35	531.5
3.5	959.12	534
4	958.9	536
4.5	958.55	539
5	958.2	541

Table 2. Comparison between detected power at positive phase shifts and their equal negative phase shifts at basic and phase modulated FOGs.

Phase Shift (deg)	Detected Power for Basic FOGs Configuration (uW)	Detected Power for Phase Modulation FOGs Configuration (uW)
10	952.7	562.16
-10	952.7	473.5
20	931.05	604.3
-20	931.05	429.7
30	895.69	643.3
-30	895.69	388.03

45	819.41	693.3
-45	819.41	332.3
90	480	755.3
-90	480	244.7

4.2. Phase modulated FOGs configuration

Figure 6 illustrates the simulation of a phase modulated FOGs, mirroring the basic configuration after applying the phase modulators driven by sinusoidal generators as additional components within the configuration. Setting the modulation depth to 0.9 and appropriately adjusting the frequency of the sine generator, the zero-point illustrated in figure 2 - indicating no rotation - was shifted from the position of maximum detected power to a point where the graph exhibits the maximum slope. This adjustment was crucial in enhancing sensitivity and facilitating the detection of the rotation's direction within the system. In figure 7, the anticipated outcome is observed: the zero point has indeed shifted to the region of high slope within the graph, precisely as anticipated and discussed earlier. This shift signifies the successful resolution of the two problems previously mentioned, showcasing how this method effectively addresses the issues encountered in the basic configurations of the system.

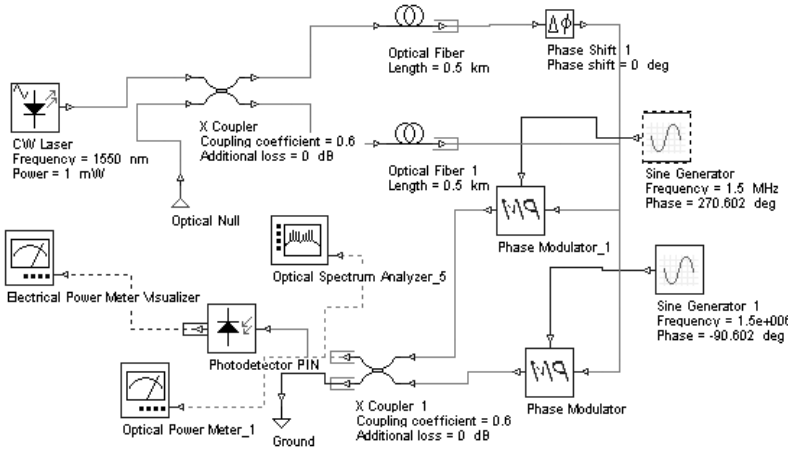

Figure 6. Simulation of Phase Modulated FOGs Configuration

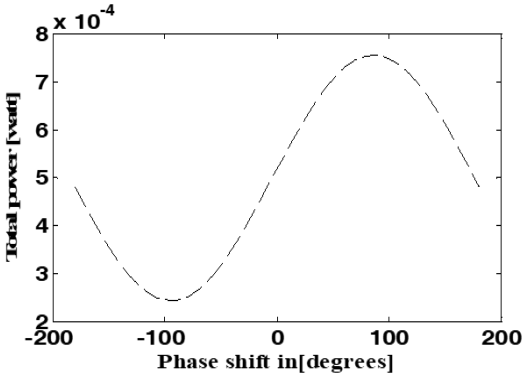

Figure 7. Simulation result of Relation between Phase Shift and Detected Power for Phase Modulated FOGs Configuration

Thus, by comparing the detected power readings for the same phase shifts from Table 1 within the phase modulated FOGs, it becomes apparent that very low rotation rates no longer exhibit the same output detected power as observed in the near-zero rotation rate detection. This variance

indicates an improvement in sensitivity within the phase modulated configuration, resolving the low sensitivity issue encountered in the basic configurations.

Also, Table 2 indicates that within the phase modulated FOGs, identical phase shifts with different signs no longer yield the same detected power, which was an issue in the near-zero rotation rate setup mentioned before. This change signifies the successful resolution of the problem related to discerning the direction of rotation within the phase modulated configuration, showcasing its ability to distinguish between rotations of opposite directions.

5. Conclusion

In this work we introduced an approach to resolve the limitations of the near-zero rotation rate setup in Fiber Optic Gyroscopes (FOGs). Addressing the issues of low sensitivity and indiscernibility of rotation direction is a significant step forward in enhancing the functionality of inertial navigation sensors. Where, we managed to study and simulate an enhanced configuration for the FOG using a phase modulator that acts on shifting the operating region of detection from the flat region to the maximum slope region within the relation between the phase shift due to the rotation rate and the detected power. Although our solution is effective in enhancing sensitivity at the near-zero rotation rate region, it limits the dynamic range, focusing primarily on the high slope area of the phase shift and detected power. To advance this technology further, future work should aim to broaden the dynamic range, ensuring it's not confined to a specific area and allowing for a more extensive range of detectable rotations. This expansion could significantly improve the overall performance and applicability of FOGs in inertial navigation and control systems.

6. References

[1]. Bergh R, Lefevre H, Shaw H. An overview of fiber-optic gyroscopes. Journal of Lightwave Technology. 1984;2(2):91–107.
[2]. Post EJ. Sagnac effect. Rev Mod Phys. 1967;39(2):475.
[3]. Lloyd SW. Improving fiber optic gyroscope performance using a single-frequency laser. Stanford University; 2014.
[4]. Lefevre HC. The fiber-optic gyroscope. Artech house; 2022.
[5]. Skalský M, Havránek Z, Fialka J. Efficient modulation and processing method for closed-loop fiber optic gyroscope with piezoelectric modulator. Sensors. 2019;19(7):1710.
[6]. Prilutskii VE, Ponomarev VG, Marchuk VG, Fenyuk MA, Korkishko Yu N, Fedorov VA, et al. Interferometric closed-loop fiber optic gyrocopes with linear output. In: Proc 5th Pacific Rim Conf on Lasers and Electro-Optics. 2003.
[7]. Jin J, He J, Song N, Ma K, Kong L. A compact four-axis interferometric fiber optic gyroscope based on multiplexing for space application. Journal of Lightwave Technology. 2020;38(23):6655–63.
[8]. Korkishko YN, Fedorov VA, Prilutskii VE, Ponomarev VG, Marchuk VG, Morev I V, et al. Fiber optical gyroscope for space applications. In: Optical Fiber Sensors. Optica Publishing Group; 2006. p. TuE91.
[9]. Juang JN, Radha Ramanan R. Evaluation of ring laser and fiber optic gyroscope technology. School Of Engineering, Mercer University, Macon, GA. 2009;31207:1–9.
[10]. Lee B. Review of the present status of optical Fiber sensors. Optical Fiber technology. 2003;9(2):57–79.
[11]. Zhang D, Liang C, Li N. A novel approach to double the sensitivity of polarization maintaining interferometric fibre optic gyroscope. Sensors. 2020;20(13):3762.
[12]. Nayak J. Fiber-optic gyroscopes: from design to production. Appl Opt. 2011;50(25):E152–61.
[13]. LEFÈRE HC. Fundamentals of the interferometric fiber-optic gyroscope. Opt Rev. 1997;4(1A):20–7.

[14]. Pavlath GA. Fiber optic gyros past, present, and future. In: OFS2012 22nd International Conference on Optical Fiber Sensors. SPIE; 2012. p. 53–62.